Supplemental materials

The Supplemental materials contain:
1. Supplemental movies 1-5
2. Supplemental table 1
3. Supplemental notes
4. Supplemental figures S1-S8 with figure captions
5. Supplemental experimental procedures

Supplemental movies

Each movie shows the sequence of images acquired at 5 Hz via widefield imaging of the olfactory bulb (OB) in response to 12 s pulse of odor. Odor presentation was flanked by clean air periods (12 s) both before and after. For visualization purpose, the baseline fluorescence (average of pre odor frames) was subtracted from each frame. The frame rate is sped up 10 times. Specific details for each movie are listed below.

Supplemental movie 1 - related to Figure 1

Responses from a DAT-Cre mouse crossed to Ai38 (ROSA-LoxP-STOP-LoxP-GCaMP3.0) upon presentation of Isoamyl acetate. Odor was diluted 1:10,000 times in mineral oil.

Supplemental movie 2 - related to Figure 1

Responses from a DAT-Cre mouse crossed to Ai38 (ROSA-LoxP-STOP-LoxP-GCaMP3.0) upon presentation of Isoamyl acetate. Odor was diluted 1:100 times in mineral oil.

Supplemental movie 3 - related to Figure 1

Responses from a DAT-Cre mouse crossed to Ai38 (ROSA-LoxP-STOP-LoxP-GCaMP3.0) upon presentation of 2-heptanone. Odor was diluted 1:100 times in mineral oil.

Supplemental movie 4 - related to Figure 1

Responses from a TH-Cre mouse injected with AAV2.9-DIO-GCaMP3.0 upon presentation of 2-heptanone. Odor was diluted 1:10,000 times in mineral oil.

Supplemental movie 5 - related to Figure 1

Responses from a TH-Cre mouse injected with AAV2.9-DIO-GCaMP3.0 upon presentation of Heptanal. Odor was diluted 1:100 times in mineral oil.

Supplemental Table 1: Odor Lists - related to Figure 1, 2, and 7.

Supplemental notes – related to Figure 1 and Figure 6

Control experiments concerning the spatial extent of the widefield odor signals.

We wanted to verify that the large spatial extent of the diffuse signals was not due to light scattering. To do so, we imaged OMP-SpH mice (Bozza et al., 2004), which express a fluorescent reporter of presynaptic release (synapto-pHluorin, SpH) in OSN terminals. SpH responses were spatially localized with sharp boundaries as indicated by single-pixel correlation analysis (**Figure 1I** and **S2C-F**) in contrast to the widespread GCAMP3.0 signals in DAT+ cells throughout the bulb surface (**Figure S2G-I**).

A recent study that monitored SA cell responses by targeting GCaMP3.0 expression to TH+ neurons reported only focal responses (Wachowiak et al., 2013). In contrast, we also observed widespread odor responses in TH-Cre mice (**Figure S2J-L, Supplemental movies 4-5**). Given the smaller amplitude of the diffuse component as compared to the focal component of the odor responses, differences in threshold criteria for signal detection and/or in the optical configuration may explain the observed difference.

We hypothesized that the widespread response results from activation of the long-range processes of DAT+ cells associated with only a few odor-activated glomeruli. To confirm this hypothesis, we focally expressed GCaMP3.0 in DAT+ cells and imaged neuropil responses in regions distal to the injection site (>1 mm away), where no labeled cell bodies were found (**Figure S1A** and **S3A-B**). Two-photon imaging of neuropil revealed sparse and odor-specific responses similar to DAT+ cell bodies (**Figure S3B-C** and **2B-E**). In contrast, wide-field imaging of GCaMP3.0 signals in the same OB showed focal activity patterns exclusively near the injection site and diffuse signals as far as 1 mm away. We conclude that calcium responses from DAT+ cell neuropil underlie the diffuse component of the widefield signal (**Figure S3D**).

In-vitro whole cell recordings to probe synaptic and electrical connections between DAT+ and M/T cells.

In-vivo pharmacological experiments suggested the possibility of electrical coupling between DAT+ and M/T cells (**Figure 5**), with the caveat that the synaptic block was not complete (**Figure S6D**). Therefore, to investigate the interaction between DAT+ cells and M/T cells under controlled experimental conditions, we performed whole cell recordings from mitral cells in acute bulb slices from DAT-Cre mice injected with AAV2.9-DIO-ChR2-EYFP or crossed to Ai32 mice. We confirmed in wild-type mice that light stimulation intensities used in all subsequent experiments did not evoke any significant current in recorded mitral cells or ET cells *in vitro* (**Figure S7C-E)**. Full-field stimulation of ChR2-expressing DAT+ cells did not produce an outward current in M/T cells in voltage clamp, but reduced the number of EPSCs in current clamp (**Figure S8A-C)**, resulting in an apparent outward current when averaged across trials (**Figure S8C**). The absence of direct synaptic inhibition onto M/T cells is consistent with a recent study (Whitesell et al., 2013). We also did not observe any light-induced inward currents

after the application of synaptic blockers (**Figure S8C-ii**). These results argue against a direct synaptic or electrical connection between DAT+ cells and M/T cells.

Figure S1: related to Figure 1

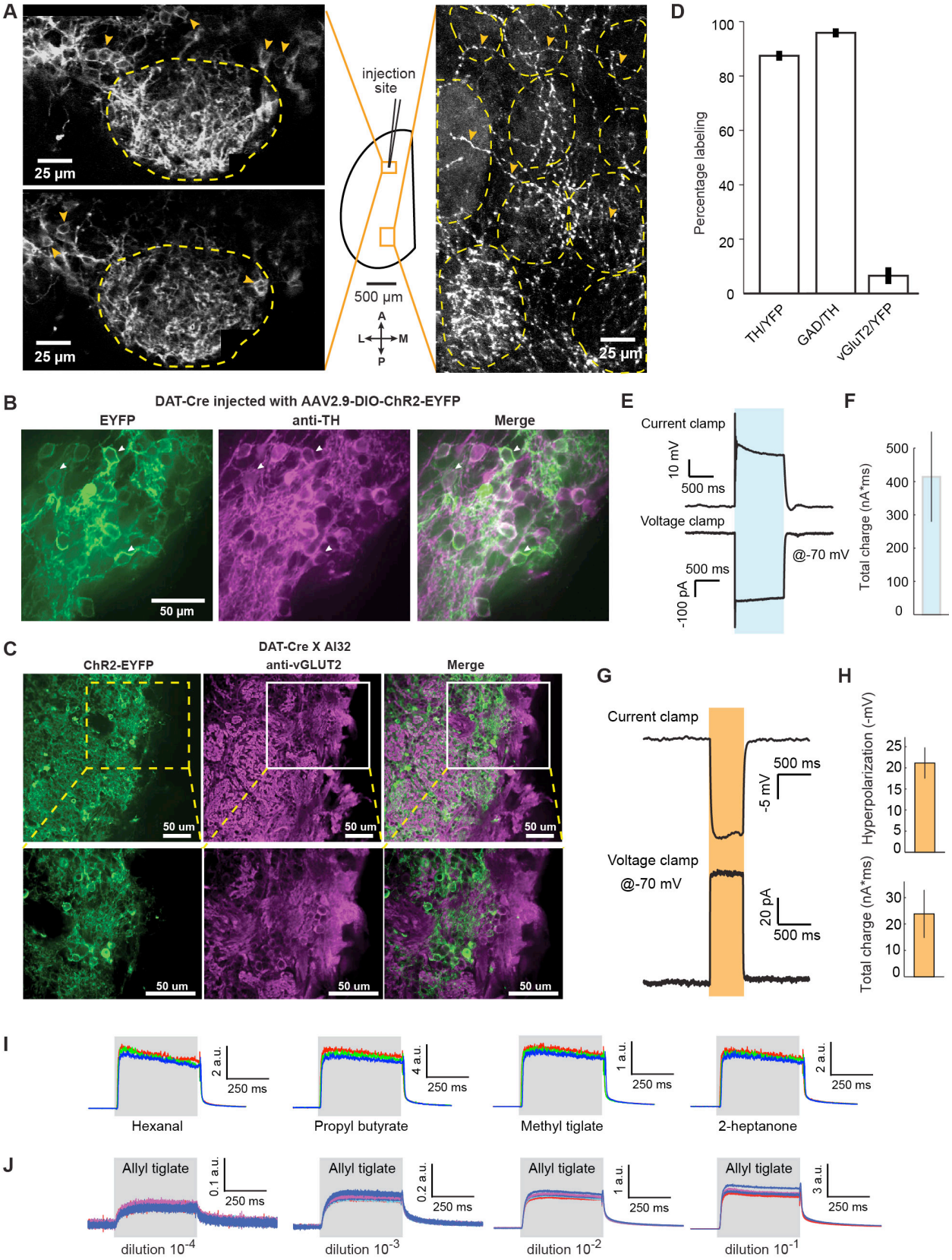

Figure S1: Histochemical, anatomical and optogenetic characterization of DAT+ cells.

A) *In vivo* two-photon projection images of fields of view (FOVs) imaged close and far away from the AAV2.9-DIO-ChR2-EYFP virus injection site. Dashed lines mark outlines of visually identified glomeruli throughout the z-stack. Fiduciary marks indicate a few example DAT+ cell bodies.

B) Confocal images of sagittal bulb slices from a DAT-Cre mouse injected with AAV2.9-DIO-ChR2-EYFP showing ChR2-EYFP fluorescence (*left*) and immunolabeling with a TH antibody (*center*). *Right*, Pseudo-colored merge of EYFP (green) and anti-TH (magenta) staining showing co-expression of TH in targeted neurons. Fiduciary marks show individual cell bodies.

C) Confocal images of sagittal bulb slices from a DAT-Cre X Ai32 mouse showing ChR2-EYFP fluorescence (*left*) and immunolabeling with anti vGLUT2 antibody (*center*). *Right*, Pseudo-colored merge of EYFP (green) and anti-vGLUT2 (magenta) staining showing insignificant co-expression.

D) Percentage of co-labeled cells in various dual and triple immunolabeling experiments. Numbers indicate mean +- SEM (total cell count TH/YFP: n = 226, GAD/TH: n = 118, vGlut2/YFP: n = 115).

E) Example current clamp (*top*) and voltage clamp (*bottom*) traces (average of 10 repeats) from a ChR2-EYFP expressing DAT+ cell upon 1 s of blue light stimulation.

F) Summary of total light-induced charge for 6 ChR2-EYFP expressing DAT+ cells.

G) Example current clamp (*top*) and voltage clamp (*bottom*) traces (average of 10 repeats) from a NpHR3.0-EYFP expressing DAT+ cell upon 0.5 s of red light stimulation.

H) Average hyperpolarization (*top,* across 9 cells) and total charge (*bottom,* across 7 cells) induced in DAT+ cells expressing NpHR3.0-EYFP.

I) PID traces for interleaved presentations of 4 odors (3 repeats). Colors indicate individual trials. All odors at 10^{-2} dilution in mineral oil. PID output is represented in arbitrary units (a.u.).

J) PID traces for increasing concentrations of a representative odor - Allyl tiglate. Odor concentrations are reported as nominal dilutions in mineral oil. Colors indicate individual trials (5 repeats). PID output is represented in arbitrary units (a.u.).

Figure S2: related to Figure 1 and Figure 2

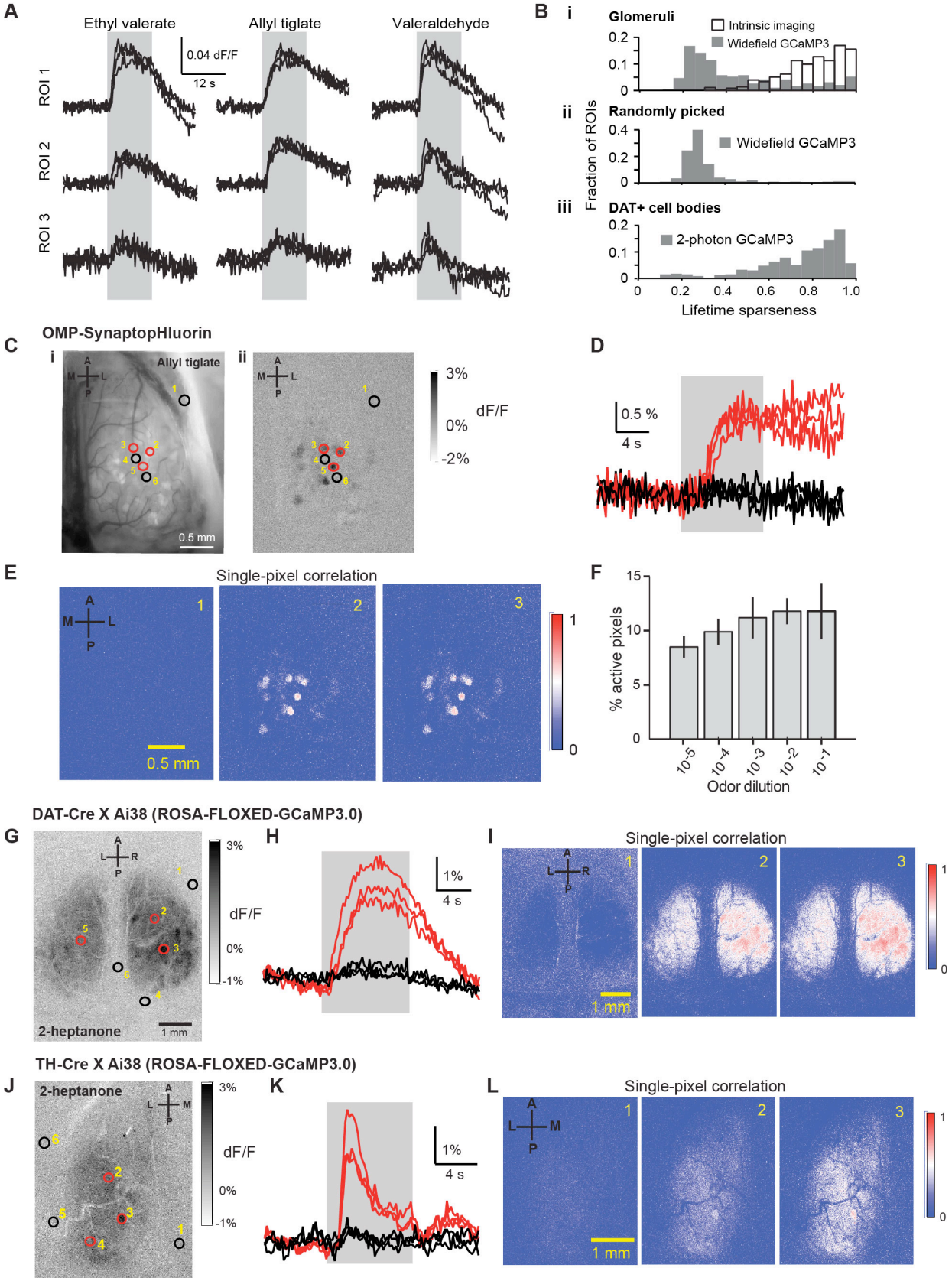

Figure S2: Characterization of widefield odor responses of DAT+ cells.

A) Baseline-subtracted, normalized widefield GCaMP3.0 signals (dF/F) from 3 glomerular ROIs on the bulb surface in response to Ethyl valerate, Allyl tiglate and Valeraldehyde. All odors at 10^{-2} nominal dilution in mineral oil. Black traces indicate individual trials. Gray band indicates odor presentation.

B) Distributions of lifetime sparseness of ROIs chosen by IOI, widefield and two-photon GCaMP3.0 odor responses of DAT+ cells. (***i***) Lifetime sparseness of intrinsic optical imaging (IOI) (empty black bars, 347 ROIs, 5 bulbs) and widefield GCaMP3.0 responses (gray bars, 188 ROIs, 3 bulbs, 3 mice) of all glomerular ROIs. Glomerular ROIs were chosen using glomerular outlines obtained from IOI. Numbers indicate mean ± SEM. (***ii***) Lifetime sparseness of GCaMP3.0 responses of randomly chosen glomerular size ROIs (gray bars, 347 ROIs, 5 bulbs, 3 mice). (***iii***) Lifetime sparseness of two-photon GCaMP3.0 responses of DAT+ cell bodies (gray bars, 331 ROIs, 4 mice).

C) Widefield image showing resting (*left*) and odor-evoked (dF/F image, *right*, Allyl tiglate, 10^{-1} dilution) fluorescence in the exposed olfactory bulb of an OMP-SpH (+/-) mouse. Open circles indicate six randomly chosen glomerular size ROIs on the exposed bulb surface. Red circles correspond to ROIs drawn over responsive glomeruli. Black circles correspond to ROIs drawn over non-responsive glomeruli, or bone. Numbers indicate ROI index.

D) Average responses of ROIs shown in **C**, upon presentation of Allyl tiglate (10^{-1} dilution). Each trace represents the average change in fluorescence (3 repeats) with respect to pre-odor baseline. Colors indicate ROIs selected on bulb surface (red) and bone (black) respectively.

E) Color maps showing correlation of the average odor-evoked response of each pixel with a given reference pixel chosen from the first three ROIs shown in **C.** ROI index of the glomerular ROI used to choose the reference pixel is indicated in the top right corner of each color map.

F) Average spatial spread of SpH responses as a function of increasing odor concentration. Each bar shows average for all bulb-odor pairs (dilutions 10^{-5} to 10^{-1}: 2 bulbs, 7 odors). Error bars indicate SEM. Odor concentrations are reported as nominal odor dilutions in mineral oil.

G) Widefield image showing odor-evoked (dF/F image, 2-heptanone, 10^{-2} dilution) GCaMP3.0 fluorescence in the exposed olfactory bulb of DAT-Cre x Ai38 reporter mouse line. Open circles indicate six randomly chosen glomerular size ROIs on the exposed bulb surface (red) and bone (black). Numbers indicate ROI index.

H) Average response of the ROIs shown in **G**, in response to 2-heptanone (10^{-2} dilution). Each trace represents the average change in fluorescence (3 repeats) with respect to pre-odor baseline. Colors indicate ROIs selected on bulb surface (red) and bone (black) respectively.

I) Color maps showing correlation of the average odor-evoked response of each pixel with a randomly chosen reference pixel from each of the first three glomerular ROI shown in **G**. ROI index of the glomerular ROI used to choose the reference pixel is indicated in the top right corner of each color map.

J) Odor-evoked GCaMP3.0 fluorescence in an example hemi-bulb from a TH-Cre mouse injected with DIO-GCaMP3-AAV2.9 in response to 2-heptanone (10^{-2} dilution). Open circles indicate six randomly chosen glomerular size ROIs on the exposed bulb surface (red) and bone (black). Numbers indicate ROI index.

K) Average response of ROIs shown in **J**. Each trace represents the average change in fluorescence (3 repeats) with respect to pre-odor baseline. Colors indicate ROIs selected on bulb surface (red) and bone (black) respectively.

L) Color maps showing correlation of the average odor-evoked response of each pixel with a given reference pixel chosen from the first three glomerular ROI shown in **J**. ROI index of the glomerular ROI used to choose the reference pixel is indicated in the top right corner of each color map.

Figure S3: related to Figure 2

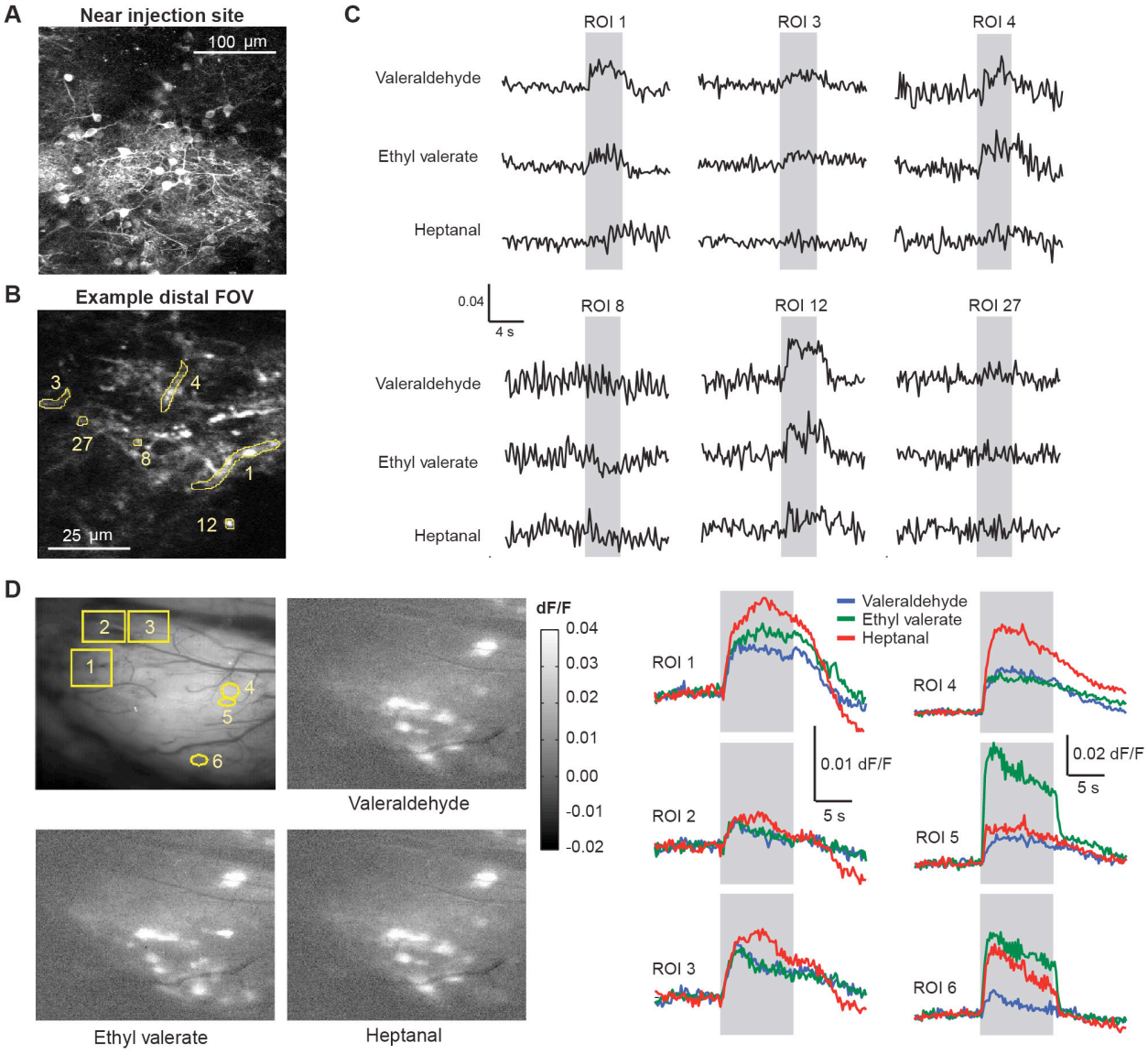

Figure S3: Two-photon and widefield odor signals from DAT+ cell neuropil.

A) Maximum projection image of a z-stack proximal to the focal injection site showing dense labeling of DAT+ cell bodies.

B) Image of an example field-of-view (FOV) far from the injection site (> 1.5 mm) averaged over 100 frames at 5 Hz. Six regions of interest (ROIs) were chosen on the neuropil of DAT+ cells, including a few boutons. No DAT+ cell bodies were observed this far from the injection site.

C) Average baseline subtracted normalized responses (dF/F) of six representative neuropil ROIs (as indicated on **B**) to three odors - Valeraldehyde, Ethyl Valerate and Heptanal.

D) Widefield GCaMP3 odor signals (dF/F) from three ROIs (4, 5 and 6) selected near the injection site and three ROIs (1, 2 and 3) selected far from the injection site. Distinct glomeruli were activated near the injection site for the three odors - Valeraldehyde, Ethyl valerate and Heptanal. No activated glomeruli were seen in the anterior aspects of the same OB as above, far from the injection site. However, the three ROIs (1, 2 and 3) far from the injection site showed robust GCaMP3 signals to all the three odors.

Figure S4: related to Figure 3

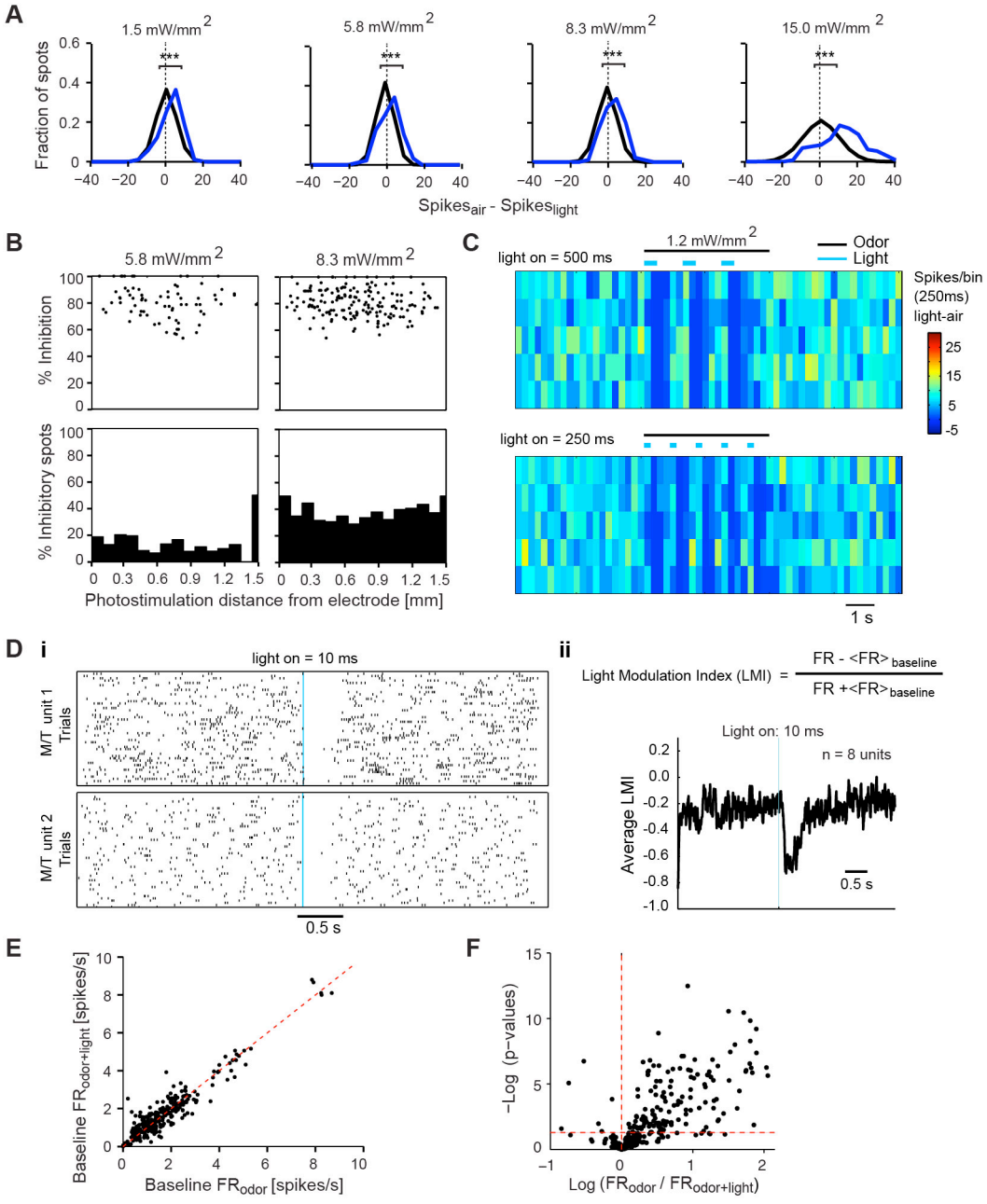

Figure S4: Effects of photoactivating DAT+ cells on M/T cell firing.

A) Distribution of difference in spike counts (Δ spikes) of the recorded M/T unit (shown in **Figure 3B**), upon photostimulation of individual light spots, compared to pre-stimulation period at various light intensities (1.5, 5.8, 8.3, 15 mW/mm^2). Blue line shows the experimentally observed distribution. Black line shows distribution of differences between independent sets of randomly shuffled pre-stimulation periods. At all light intensities, the experimentally obtained distribution was significantly right-shifted compared to the shuffled control, indicating light-induced inhibition. Paired t-test, *** denote $p < 0.001$.

B) *Top*, Strength of light-evoked inhibition as a function of photostimulation distance from the recording site for all M/T units at two light intensities (5.8 mW/mm^2 n = 5, 8.3 mW/mm^2 n = 4). Each dot represents evoked-inhibition upon stimulation of an individual spot. Only spots that evoked a significant change from baseline are plotted (two-sample t-test, $p < 0.05$). *Bottom*, Fraction of significantly inhibited spots as a function of photostimulation distance from the recoding site (two-sample t-test, $p < 0.05$) at two light intensities (5.8, 8.3 mW/mm^2). Each dot/bar denotes average of all spots from all recorded M/T units at the respective photostimulation distance and light intensity.
C) Baseline subtracted PSTH of an M/T cell upon full-field blue light activation of DAT+ cells for 500 ms (*top*) and 250 ms (*bottom*). The black and blue lines indicate odor and light stimulation respectively.
D) (*i*) Raster-plot of two M/T cell units upon full-field blue light activation of DAT+ cells for 10 ms. Each row represents an individual trial. The blue bar denotes the light-on period. **(*ii*)** Average Light Modulation Index as a measure of light induced suppression of M/T cell spontaneous activity (n = 8 M/T units, 2 mice) for 10 ms light activation of DAT+ cells. Light Modulation Index was calculated as the normalized difference in firing rate (FR) between every 5 ms bin and the average baseline FR. The plot has been smoothened with a 5 ms sliding window. The blue bar denotes the light-on period.
E) Scatter plot of average baseline firing rates of individual M/T units preceding the 'odor' and 'odor + light' conditions. Diagonal unity line marks slope of 1, indicating no change in firing rate; 351 pairs, 41 M/T units from 6 mice.
F) Volcano plot of light-induced change in odor-evoked firing of individual M/T units (FR odor / FR odor+light) and p-values obtained from a two-sample t-test. All values are plotted on log scale. Solid red line indicates p-value cutoff for significant change in firing ($p < 0.05$). Quadrants *left* and *right* of the dotted red line indicate light-induced excitation and inhibition respectively.

Figure S5: related to Figure 4

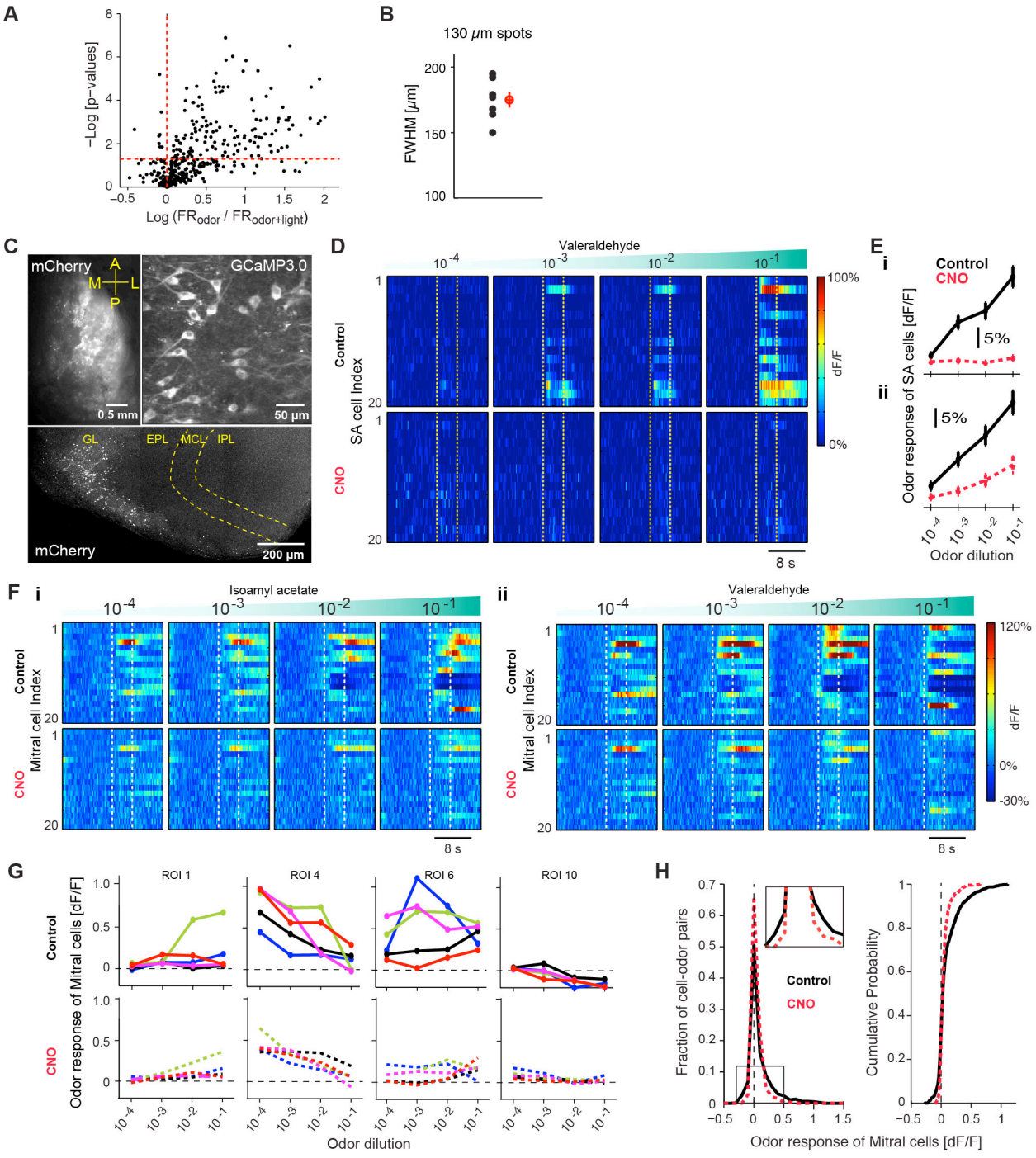

Figure S5: Optogenetic and phamacogenetic silencing of DAT+ cells suppresses M/T odor responses.
A) Effect of silencing NpHR3.0 expressing DAT+ cells. Volcano plot of light-induced change in odor-evoked firing of individual M/T units (FR odor / FR odor+light) and p-values obtained from a two-sample t-test. All values are plotted on a log scale. Horizontal red line indicates p-value cutoff for significant change in firing ($p < 0.05$). Quadrants *left* and *right* of the vertical red line indicate light-induced excitation and inhibition respectively.

B) Summary of estimated full-width-at-half-maxima (FWHM) of 'cold-spots' obtained (see **Figure 4D**) by fitting a normalized Gaussian distribution across 7 M/T units from 2 mice. Error bar denotes standard error of the mean. FWHM = 175±5.9 μm, n = 7 cells.

C) Images from the olfactory bulb of a DAT-Cre x Ai38 mouse injected with AAV2.9-DIO-DREADDi-mCherry virus in the glomerular layer, and with PRV-Cre in the piriform cortex. *Top, Left*: widefield image showing mCherry expression in the exposed olfactory bulb; *Top, Right: In vivo* two-photon image of resting fluorescence showing GCaMP3.0 expression in M/T cells. *Bottom*, confocal image showing selective expression of mCherry only in the glomerular layer.

D) Baseline-subtracted, normalized GCaMP3.0 signals from an example imaging session of DAT+ cell responses to increasing concentrations of heptanal before (control, *Top*) and after CNO injection (*Bottom*). Stimulus concentrations are reported as nominal dilution in mineral oil. Each row represents an individual DAT+ cell (ROI) in the same field of view. Color indicates normalized change in fluorescence with respect to pre-odor baseline (dF/F). Dotted lines indicate odor presentation (4 s). Images were acquired at 5 Hz.

E) (***i***) Average odor-evoked response (dF/F) of all DAT+ cells (20 ROIs) shown in **D**, across five odors as a function of increasing odor concentration. Black and red (dotted) lines show responses before and after CNO injection. Error bars indicate standard error of mean. ***(ii)*** Average odor-evoked response (dF/F) of all responsive DAT+ cells (110 cells, 3 mice), across five odors as a function of increasing odor concentration. Black and red (dotted) lines show responses before and after CNO addition. Error bars indicate SEM.

F) Baseline-subtracted, normalized GCaMP3.0 signals from an example imaging session of M/T cells to increasing concentrations of Isoamyl acetate (*i*) and Valeraldehyde (*ii*) before (control, *Top*) and after (CNO, *Bottom*) CNO injection. Stimulus concentrations are reported as nominal dilution in mineral oil. Each row represents an individual M/T cell (ROI). Color indicates relative change in fluorescence with respect to pre-odor baseline (dF/F). Dotted lines indicate odor presentation. Images were acquired at a frame rate of 5 Hz.

G) Average odor-evoked response (dF/F, 2-3 repeats) of four example M/T cells (ROIs) shown in **F**, to five odors, as a function of increasing odor concentration, before (control, solid lines, *Top*) and after (CNO, dotted lines, *Bottom*) CNO injection. Colors indicate individual odors (same as **Figure 2G**).

H) Summary histogram (*Left*) and cumulative distribution (*Right*) of M/T odor responses as a function of normalized response strength (dF/F) before (black) and after (red) CNO injection. 49 cells, 842 cell-odor pairs, 3 mice.

Figure S6: related to Figure 5

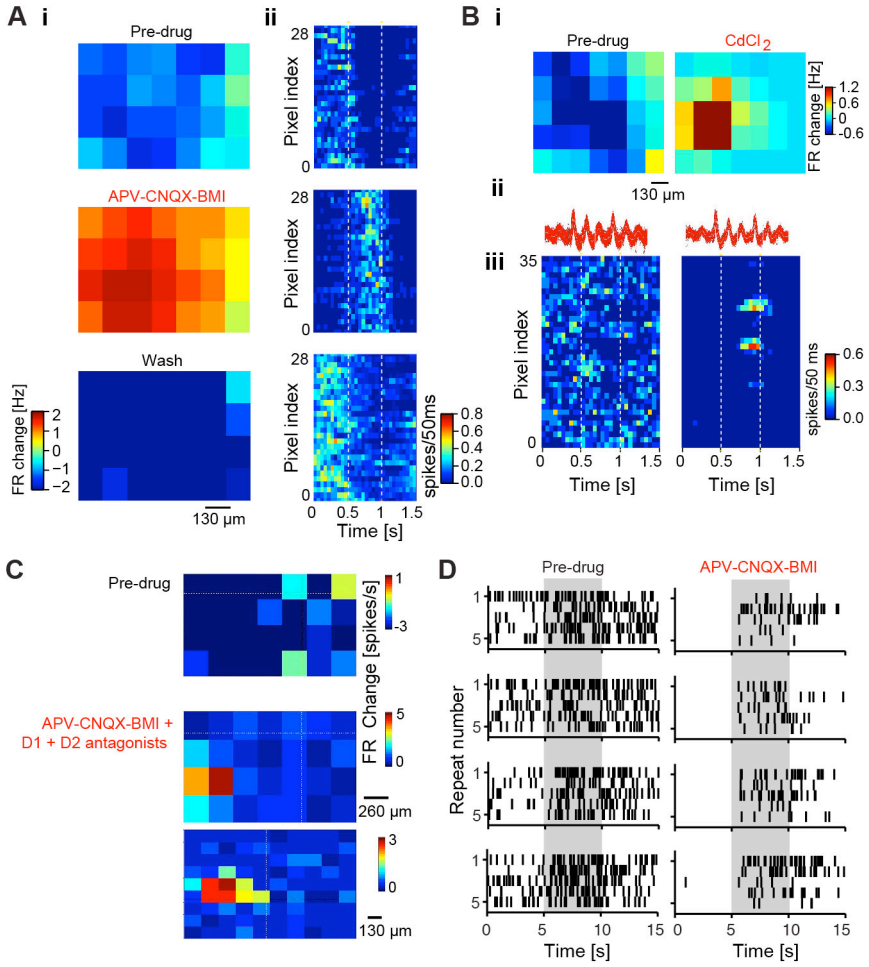

Figure S6: Light-induced suppression of M/T cells by DAT+ cells switches to excitation in presence of synaptic blockers.

A) (*i*) 2D light map from a DAT-cre mouse injected with AAV2.9-DIO-ChR2-EYFP virus, showing change in firing of an example M/T unit upon random mapping of the bulb surface with blue light spots (130 μm X 130 μm, 15 mW/mm^2) before (*top*), during blocking synaptic transmission via APV-CNQX-BMI (*middle*) and post-wash (*bottom*) of the drug cocktail. Color indicates average firing rate (FR) change in M/T spiking with respect to pre-light stimulation baseline. **(*ii*)** PSTH of all spots from the same light mapping session in **(*i*)**, before (*top*), during (*middle*) and post-wash (*bottom*) drug application. Pixels, from *bottom left to top right corner*, in the light map are re-ordered as *top to bottom rows* in the PSTH. Dotted lines indicate the photostimulation period. Color indicates firing rate in 50 ms bins.

B) (*i*) 2D light maps from a DAT-cre mouse injected with AAV2.9-DIO-ChR2-EYFP virus before (*left*) and during (*right*) application of $CdCl_2$. **(*ii*)** Spike waveforms of the M/T unit in **(*i*)** before (*left*) and during (*right*) application of $CdCl_2$. **(*iii*)** PSTH of all spots for an example M/T unit, upon random mapping of the bulb surface with blue light spots (130 μm X 130 μm, 15 mW/mm^2) before (*left*) and during (*right*) $CdCl_2$.

C) 2D light maps from a DAT-cre mouse injected with DIO-ChR2-EYFP AAV virus before (*Top*) and during (*Middle, Bottom*) application of APV-CNQX-BMI + D1 and D2 receptor antagonists (SKF83566 hydrobromide, sulpiride). *Top and middle* light maps show change in firing rate of an example M/T unit, upon random mapping of the bulb surface with blue light spots (260 μm X 260 μm, 15 mW/mm^2). Bottom light map shows change in firing

rate of the same M/T unit, upon random mapping of the bulb surface with smaller blue light spots (130 μm X 130 μm, 15 mW/mm^2, 3 M/T units, 2 mice).

D) Raster of an example M/T unit to four odors (from *top* to *bottom*: Allyl tiglate, Isoamyl acetate, Valeraldehyde, Ethyl valerate; dilution 10^{-2}) before (*left*) and after (*right*) addition of APV-CNQX-BMI. Each row represents an individual trial. Gray bar indicates duration of odor presentation.

Figure S7: related to Figure 4

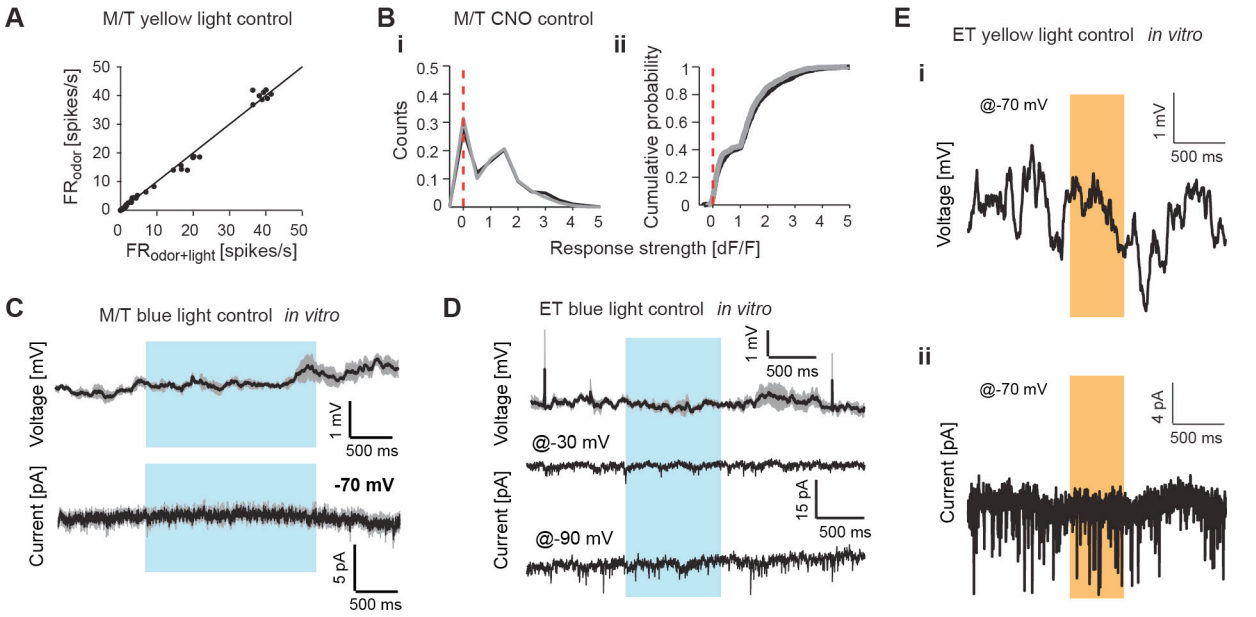

Figure S7: Optogenetic and pharmacogenetic controls in wild-type mice.

A) Scatter plot of average firing rates of M/T units during 'odor' and 'odor+light' conditions in wild-type mice upon full-field yellow light stimulation (3 mW/mm^2). Diagonal marks slope of 1, indicating no change in firing rate (5 M/T units, 35 cell-odor pairs, 3 mice).

B) Histogram (***i***) and cumulative distribution (***ii***) of M/T GCaMP3.0 odor responses as a function of normalized response strength (dF/F) before (black) and after (gray) CNO injection (51 M/T cells, 1020 cell-odor pairs, 3 mice).

C) Average current clamp (*top*) and voltage clamp (*bottom*) traces recorded from M/T cells in bulb slices of wild-type mice, upon blue light stimulation (7 mW, at the objective exit). Black line and shaded region represent mean and SEM (3 cells).

D) Average current clamp (*top*) and voltage clamp (*middle, bottom*) traces recorded from ET cells in bulb slices of wt mice, upon blue light stimulation (7 mW, at the objective exit). Black line and shaded region represent mean and SEM (3 cells in current clamp, 2 cells in voltage clamp).

E) Current clamp (***i***) and voltage clamp (***ii***) (holding potential of -70 mV) traces recorded from an ET cell in bulb slices of wt mice, upon red light stimulation (0.8 mW/mm^2).

Figure S8: related to Figure 6

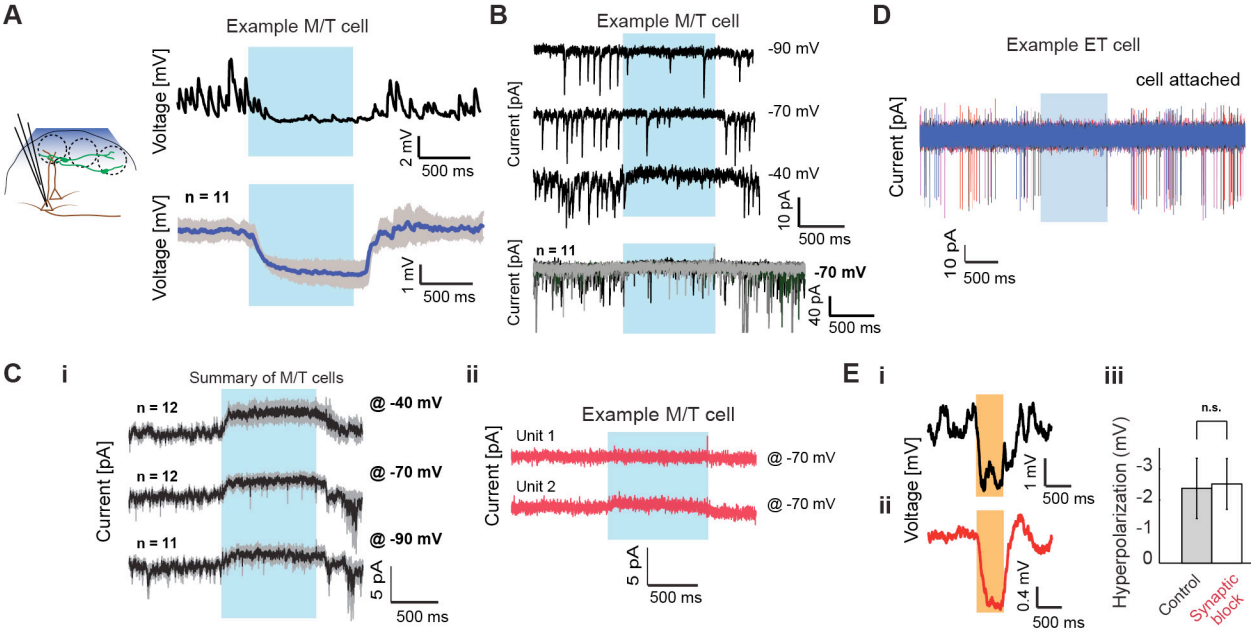

Figure S8: Whole-cell recordings from Mitral cells and ET cells during optogenetic manipulations of DAT+ cells

A) *Left*: Schematic of the experiment. *Top*, *Right*: Light-induced hyperpolarization in an example current clamp trace from a M/T cell upon full-field blue light stimulation (1 s) of ChR2-expressing DAT+ cells in an acute horizontal olfactory bulb slice. Black trace shows an individual trial. Blue bar marks duration of light stimulation. *Bottom, Right*: Mean light-induced hyperpolarization across 10 M/T cells upon optogenetic activation (1 s) of DAT+ cells (blue trace). Shaded gray region shows SEM.

B) *Top*, Example voltage clamp traces showing light-induced reduction of EPSCs frequency in the example M/T cell shown in **A** upon ChR2 stimulation (1 s) of DAT+ cells at three different holding potentials. Black traces show individual trials. Blue bar marks the duration of light stimulation. *Bottom*, Individual voltage-clamp traces from 11 M/T cells recorded at -70 mV holding potential. Blue bar marks duration of light stimulation.

C) (*i*) Average light-induced current trace from mitral cells at three different holding potentials (-40 mV, -70 mV: n = 12 cells; -90 mV: n = 11 cells). Gray shaded region represent the SEM. Blue bar marks duration of light stimulation. **(*ii*)** Average light-induced current trace from two mitral cells at -70 mV holding potential (10 repeats) in the presence of synaptic blockers (NBQX, APV, picrotoxin, S-(-)-eticlopride hydrochloride and SKF83566).

D) Superposition of 10 voltage clamp traces from an example ET cell recorded in the cell-attached configuration, showing suppression of spontaneous firing upon blue light stimulation. Colors indicate individual trials.

E) Light-induced voltage trace (average of 10 trials) from an example ET cell in control conditions **(*i*)** or in the presence of synaptic blockers **(*ii*)**. Summary of average hyperpolarization induced in ET cells upon inactivation of NpHR3.0 expressing DAT+ cells before (n = 8 ET cells) or after synaptic blockers (n = 5 ET cells). They are not significantly different (p-value = 0.93, two-sample t-test).

Supplemental Experimental Procedures

Surgical Procedures

Adult mice (males and females >30 days old, 25-40 g) were anesthetized with ketamine/xylazine (KX, initial dose 70/7 mg/kg), further supplemented via a peristaltic pump (Harvard Apparatus, Pump 11 Plus) and maintained between 40-70 mg/kg throughout the experiment. Temperature was maintained at 37° C using a heating pad (FST TR-200, Fine Science Tools, USA). Respiratory rate and lack of pain reflexes were monitored throughout the experiment. Mice were head-fixed to a thin metal plate with acrylic glue. The skull was thinned using a high-speed dental drill (Foredom, Bethel, CT) and removed completely to reveal the dorsal surface of both bulb hemispheres. For electrophysiological recordings, the dura was removed using a pair of fine forceps. The craniotomy was filled with a thin layer of low melting point agarose (~1.2-1.5%). Cortex buffer was perfused continuously using a perfusion pump (ColePalmer Masterflex C/L). For imaging experiments, a glass cover slide was placed atop to prevent drying and to reduce motion artifacts. All animal procedures conformed to NIH guidelines and were approved by Cold Spring Harbor Laboratory Animal Care and Use Committee.

Transgenic mice

Ai9: ROSA:LoxP-STOP-LoxP:tdTomato
Ai32: ROSA:LoxP-STOP-LoxP:ChR2-EYFP
Ai38: ROSA:LoxP-STOP-LoxP:GCaMP3.0

Virus injections

DAT-Cre mice (males and females; >30 days old) were anesthetized as described above before being placed in a stereotactic frame. To express GCaMP3.0, ChR2 or NpHR3.0, AAV2.9-EF1a-DIO-GCaMP3.0 (UNC Vector core; $4X10^{12}$ viral particles/ml), AAV2.9-EF1a-DIO-ChR2-EYFP (UNC Vector core; $4X10^{12}$ viral particles/ml) and AAV2.9-EF1a-DIO-NpHR3.0-EYFP (UNC Vector core; $8X10^{12}$ viral particles/ml) were injected respectively. To express inhibitory DREADD (Designer Receptor Exclusively Activated by Designer Drugs) in DAT+ cells, AAV2.9-CAG-DIO-hM4Di-mCherry (gift from M. Luo, National Institute of Biological Sciences, Beijing; custom made AAV2.9 virus by UNC Viral Core) was injected in DAT-Cre or DAT-Cre X AI38 (ROSA-LoxP-STOP-LoxP-GCaMP3.0) mice. To express Diphteria Toxin Receptor (DTR) specifically in DAT+ cells, AAV-FLEX-DTR-GFP virus (gift from T. Jessell & E. Azim, Columbia University, New York) was injected in DAT-Cre or DAT-cre X Thy1-GCaMP3.0 mice. Virus was front loaded into 5µl pipettes (VWR international 53432-706) using a 20 ml syringe connected via a rubber tube. Virus was injected at roughly 30 nl/min by applying pressure using the syringe while visually monitoring the fluid in the pipette. To achieve uniform expression, injections were done at 3 sites per olfactory hemi-bulb at depths of 300/200/100µm from the bulb surface. ~300nl of the respective viruses were injected at each site. Injection

protocol was standardized by post-hoc imaging of expression patterns in injected brains. For slice recordings of horizontal sections, expression of ChR2 was targeted to the glomeruli at the midline. AAV2.9-EF1a-DIO-ChR2-EYFP was injected in two antero-posterior sites located 0.5mm lateral from the midline, each at four depths (1750/1250/750/250μm), ~180 nl per depth. For sparse and localized expression, ~90 nl of AAV2.9-EF1a-DIO-ChR2-EYFP or AAV2.9-EF1a-DIO-GCaMP3.0 was injected only at one anterior or posterior site per hemi-bulb. Mice were allowed to recover for at least two weeks prior to experiments with due animal care.

Immuno-histochemistry

Mice were intra-cardially perfused with 4% Para-Formaldehyde (PFA) immediately after a lethal dose of KX cocktail anesthesia. Brains were stored overnight in 4% PFA. After a few rinses with Phosphate Buffer Saline (PBS), 50 um thick sagittal sections were cut, incubated with 1% H_2O_2 for 30 minutes and subsequently washed three times with 0.1M TRIS buffer. Slices were transferred to blocking solution (10% goat serum in 0.1 M Tris buffer with 0.1% Triton-100) for 1 hour. The blocking solution was removed and washed with 0.1M TRIS buffer three times before the primary antibody was added for 48 hours at 4° C. The primary antibody was pipetted out and slices were washed 6 times with 0.1M TRIS buffer. The secondary antibody was then added for 4 hours at 4° C. Following 6 washes in PBS, the slices were mounted with Vectashield. Images were acquired using Perkin-Elmer Spinning Disk confocal microscope and were analyzed using Volocity (Perkin-Elmer) and ImageJ (NIH, USA).

Specific primary antibodies used:
1. Tyrosine Hydroxylase (TH): Rabbit anti-Tyrosine Hydroxylase (TH) antibody (Sigma, SAB4300675; diluted 1:1,000 in 0.1M TRIS buffer).
2. Glutamate decarboxylase-67 (GAD67): Mouse anti-Glutamate decarboxylase 67 (GAD67) antibody (Millipore, MAB5406; diluted 1:1000 in 0.1M TRIS buffer).
3. Vesicular Glutamate Transporter-2 (vGluT2): Mouse anti-vesicular glutamate transporter-2 antibody (Millipore, MAB5504; diluted 1:1000 in 0.1M TRIS buffer).

Specific secondary antibodies used:
1. Goat anti-rabbit Alexa 594 (Life technologies, A11037; diluted 1:500 in 0.1M TRIS buffer).
2. Goat anti-mouse Alexa Fluor 647 (Life Technologies, A21235; diluted 1:500 in 0.1M TRIS buffer)

For dual immunolabeling experiments, rabbit anti-TH antibody and rabbit anti-GAD67 antibody were simultaneously added. Secondary antibodies for anti-TH and anti-GAD67 were conjugated to Alexa 594 and Alexa 647 respectively. 3-color images were acquired simultaneously in a spinning disk confocal microscope (Perkin Elmer).

Odor delivery

Odors were delivered using a custom-made odor machine (Dhawale et al., 2010), at a net output flow rate of 1L/min. To maintain constant flow rate, a flow-rate matched clean air stream was used in absence of odor stimulation. For large odor panels, up to 100 odors were used. Odors were diluted at 1:100 (10^{-2}) in mineral oil. For concentration series experiments under widefield (**Figure 1**), a dedicated odor machine was used with up to 6 different (1:10-1:10^6) concentrations per odor. For the two-photon imaging experiments described in **Figure 2F-I**, **7** and **S5,** a subset of five odors (Allyl tiglate, Isoamyl acetate, Valeraldehyde, Ethyl Valerate and Heptanal) were used at four concentrations (1:10-1:10^4). Odor output was characterized using a photo-ionization device (**Figure S1I-J**, Aurora Scientific). These nominal dilutions do not correspond to absolute odor concentrations. Comparison with PID measurements of saturated odor vapor indicated that the actual concentrations spanned from 0.05 % to 1.3% for the large odor panel and up to 3% for the dilution series odors.

Widefield fluorescence and intrinsic optical imaging (IOI)

LED arrays were used to shine blue light (~470 nm, Luxeon V Lumileds) for GCaMP3.0 imaging, or far red light (~780 nm, Roithner Laser Technik) for intrinsic optical imaging (IOI) on the bulb surface. Images of the OB were acquired with a Vosskühler 1300-QF CCD camera, coupled to two SLR lenses positioned front to front (Nikkor 105 mm FL, f/2.0 and either Nikkor 50 mm FL, f/1.4, or Voigtländer 35 mm FL, f/1.2) with a pixel size of 12.6 μm or of 8.7 μm, as previously described in detail (Dhawale et al., 2010). For a subset of experiments, GCaMP3.0 imaging and IOI were performed in the same animal. Fluorescence imaging and IOI were alternated across blocks of 20 odors for large odor panel experiments and across individual concentration sets. Blue light intensity was calibrated to avoid photobleaching. IOI and GCaMP3.0 signals were acquired at 25 Hz and 4 Hz respectively. Each trial consisted of 12 s of odor delivery flanked by 12 s of air on both sides. The inter-trial interval was 30 s. Each stimulus was repeated on an average 3 times. Image acquisition was controlled by custom-written software in Labview (National Instruments).

Two-photon imaging

A Chameleon Ultra II Ti:Sapphire femtosecond pulsed laser (Coherent) was used together with a custom built two photon microscope. The shortest optical path was used to bring the laser onto a galvanometric mirrors scanning system (6215HB, Cambridge Technologies). The scanning system projected the incident laser beam tuned at 930 nm through a scan lens (50 mm FL) and tube lens (300 mm FL) to backfill the aperture of an Olympus 20X, 1.0 NA objective. A Hamamatsu modified H7422-40 photomultiplier tube was used as photo-detector and a Pockels cell (350-80 BK and 302RM driver, ConOptics) as beam power modulator. The current output of the PMT was transformed to voltage, amplified (SR570, Stanford Instruments) and digitized using a data acquisition board that also controlled the scanning (PCI 6115, National

Instruments). Image acquisition and scanning were controlled by custom-written software in Labview (National Instruments).

DAT+ cell imaging: In a typical experiment, multiple fields of view of ~300 X 300 μm were sampled in the glomerular layer. Before odor delivery, a z-stack was taken for each field of view (FOV) across the glomerular layer. Glomerular outlines were visually identified from the z-stacks for assignment of DAT+ cell bodies to respective glomeruli. Once an optical plane was chosen, odors were delivered and a time sequence of 120 frames at 4 Hz (10 s air, 8 s odor, 12 s air) was acquired. The inter-trial interval was 30 s. Each odor was typically delivered 2-4 times. For the concentration series experiments, once an optical plane was chosen, a set of five odors at four concentrations (1:10-1:10^4) were delivered and time lapse data acquired for 100 frames at 5 Hz (10 s of air, 4 s of odor followed by 6 s of air). The inter-trial interval was 40 s and each stimulus was repeated 2-5 times.

Difference between TH-Cre and DAT-Cre mice.

The reported expression pattern of TH-Cre mice (Wachowiak et al., 2013) shows expression in the glomerular layer, but also in the deeper layers. In contrast, expression in DAT-Cre mice that is restricted to the glomerular layer (**Figure 1A**) and shows considerable overlap for TH antibody (**Figure 1B**). To minimize non-specific targeting of cells other than the glomerular DAT+ cells, we relied on DAT-Cre mice for most experiments reported here. Only in one subset of experiments, we monitored odor responses in TH-Cre mice to allow for direct comparison to DAT-Cre mice (**Figure S2J-L**).

Photostimulation

Custom-built rigs were used for patterned photostimulation of the olfactory bulb using a DLP projector, as described in detail elsewhere (Dhawale et al., 2010). Appropriate excitation filters (Edmund Optics NT52-532 and NT66-051) and dicroic mirrors (Chroma-530dclp and 460dcsp) were used for ChR2 and NpHR3.0 stimulation. The maximum output light intensity, measured using a power-meter (Thorlabs, PM100D), was maintained stable across all experiments. Photostimulation light masks were designed using custom-written software in Labview (National Instruments). To avoid photoelectric effect, light masks were designed to cover regions excluding the electrode. We confirmed that even at the maximum light intensity used for both ChR2 and NpHR3.0 experiments, there were no non-specific (opsin-independent) effects in wild-type CBA/CAJ mice (**Figure S7**).

Extracellular recordings

Extracellular recordings in the M/T layer of the olfactory bulb were performed using standard procedures. Briefly, gold-plated tetrodes (impedance 0.7-1.0 MOhm) were made by twisting and heat-fusing four 12.5 μm polyimide-coated nichrome wires. Two tetrodes were glued together with Loctite 420 to increase the yield of single units. In several experiments, two

octrodes were used to simultaneously record from two distinct sites within the same hemi-bulb. Electrophysiological signals were amplified (RHA1016, Intan Technologies LLC), band-pass filtered between 300 Hz and 5 kHz and digitized at 30 kHz using a custom-written software in Labview (PCI-6259, National Instruments). Single units were manually isolated using MClust (MClust-3.5, A.D. Redish). For all isolated units, less than 1% of events had inter-spike intervals (ISI) less than 2 ms. Respiration was recorded using piezo-electric stress transducers (Kent Scientific TRN0028) placed under the mouse. All spike-rasters were plotted at 1 ms resolution. Peri-stimulus time histograms (PSTH) for odor-evoked responses were binned at 500 ms and for light-mapping experiments at 50 ms.

Slice electrophysiology

Animals: DAT-Cre mice injected with AAV2.9-EF1a-DIO-ChR2-EYFP or crossed with the reporter line Ai32 (ROSA-lox-STOP-lox-ChR2, Allen Institute), and DAT-Cre mice injected with AAV2.9-EF1a-DIO-NpHR3.0-EYFP (see above) were used for optogenetic stimulation and suppression of DAT+ cells, respectively.

Slice preparation: P45-P180 mice were anesthetized with an intraperitoneal injection of KX cocktail, after brief exposure to isofluorane. Deeply anesthetized mice were perfused intracardially with ice-cold slicing solution containing (mM): $NaHCO_3$ 25, $NaPO_4$ 1.25, KCl 2.5, Choline chloride 110, ascorbic acid 11.6, Na pyruvate 3.1, glucose 25, $CaCl_2$ 0.5, $MgCl_2$ 7 (95% O_2- 5% CO_2). The animal was decapitated and the olfactory bulbs were carefully extracted and transferred to ice-cold slicing solution. Horizontal slices (300 μm) were cut using a HM 6050V vibratome (Microtom). Slices were incubated in recording solution (see below) at 32º C for 30 minutes, then at 25º C for 30 minutes. Slices were visualized under an upright Olympus microscope equipped with IR-DIC and epi-fluorescence imaging. A 5X MPlan FL objective was used for the structural visualization of the OB and identification of glomerular and mitral cell layers.

Patch clamp: Slices were incubated in a recording solution optimized to enhance ET cell intrinsic bursting (**Figure S8D**), containing (mM): NaCl 119, $NaHCO_3$ 26.2, $NaPO_4$ 1, KCl 2.5, glucose 22, $CaCl_2$ 3, $MgCl_2$ 1 (95% O_2- 5% CO_2). Experiments were performed at 30º C. Whole cell recordings were obtained with borosilicate pipettes (4-7 MΩ) filled with intracellular solution containing (mM): Kgluconate 140, KCl 10, Hepes 10, EGTA 0.1, NaCl 6.9, MgATP 4, NaGTP 0.4 (pH 7.3, 290 mOsm). Alexa 594 (14 μM) was added to the intracellular solution for visualizing the neuronal morphology (**Figure 6A**). Voltage values presented in the text are not corrected for the calculated liquid junction potential (-14 mV). Signals were recorded with a Multiclamp 700B (Axon Instruments, Molecular Devices), low-pass filtered at 10 kHz and digitized at 10 kHz with an analog-to-digital converter Digidata 1440A (Axon Instruments, Molecular devices), using Clampex 10.2 software (Axon Instruments, Molecular Devices). The health of the recorded cells was assessed throughout the duration of each experiment by monitoring the spiking output in response to pulses of current injections.

Functional expression of ChR2/NpHR3.0 in DAT+ cells was confirmed by whole cell recording of EYFP-expressing cells in acute bulb slices (**Figure S1E-H**). For optogenetic stimulation of ChR2-espressing DAT+ cells, blue light from a 470 nm LED (CoolLED pE100) was coupled to the microscope in the epi-fluorescence configuration. 1-2 s light pulses were delivered to the slice through a 60X LUMPlan microscope objective, at an output power of 7 mW measured at the exit of the objective. For optogenetic suppression of NpHR3.0-expressing DAT+ cells, red light from two 625 nm LED (Luminus, CBT-40 series) was shone onto the preparation from the side of the objective, at an angle of ~20º. The intensity at the sample was ~0.8 mW/mm^2. DAT+ cells were identified by EYFP fluorescence. Blue or red light stimulation evoked a short latency (<1 ms) inward or outward currents respectively (**Figure S1E-H**). The mitral cell layer was visually identified under IR-DIC by the characteristic laminar organization of cell bodies. ET cells were recognized as pear-shaped (≥15 μm) cell bodies positioned in the lower half of the glomerular layer with a single apical dendrite confined to a unique glomerulus. 12 of the 21 recorded ET cells displayed spontaneous spiking in cell attached or whole cell recordings. Of these, 6 cells showed a characteristic bursting firing pattern (**Figure S8D**) in cell-attached recordings. For experiments involving pharmacological manipulations, inhibitors of synaptic conductances were perfused into the recording chamber. The following concentrations were used: 2,3-dihydroxy-6-nitro-7-sulfamoyl-benzo[f]quinoxaline-2,3-dione (NBQX) 10 μM, D-(-)-2-Amino-5-phosphonopentanoic acid (D-APV) 100 μM, picrotoxin 100 μM, S-(-)-eticlopride hydrochloride 10 μM, 8-Bromo-2,3,4,5-tetrahydro-3-methyl-5-phenyl-1*H*-3-benzazepin-7-ol hydrobromide (SKF83566) hydrobromide 2 μM. S-(-)-eticlopride hydrochloride and beta-glycyrrhetinic acid were purchased from Sigma Aldrich, all other drugs from Tocris Bioscience.

Pharmacology

Drugs were superfused over the exposed bulb surface 30 minutes prior to the recording and continuously thereafter. For synaptic block experiments, a cocktail of CNQX (6-cyano-7-nitroquinoxaline-2,3-dione, AMPA receptor antagonist), APV (2*R*-amino-5-phosphonovaleric acid, NMDA receptor antagonist and BMI (Bicuculline methiodide, GABA-a receptor antagonist) or $CdCl_2$ (a blocker of voltage gated Ca^{2+} channels, therefore of synaptic release) was made in cortex buffer each at a concentration of 1mM. In a subset of the synaptic block experiments (**Figure S6C**), along with CNQX, APV and BMI, D1 antagonist SKF83566 hydrobromide and D2 antagonist Sulpiride at 1mM, (TOCRIS, USA) were also added to block dopaminergic transmission. In a different subset of experiments, drugs were washed out by continuous superfusion of cortex buffer (**Figure S6A**).

For DREADDi inactivation experiments (**Figure S5**), Clozapine-N-oxide (CNO) was used as a ligand to activate the modified muscarinic receptor. CNO (Enzo Life Sciences, USA) was diluted in saline to a concentration of 4 mg/ml. CNO was injected intra-peritoneally (IP) at a final concentration of 5-10 mg/Kg of body weight. Post-CNO imaging session started 30 minutes

after the IP injection. For genetic ablation of DAT+ cells (**Figure 7**), 400 ng of diphtheria toxin dissolved in PBS (Sigma, D0564) was administered by intraperitoneal injection.

Retrograde labeling of OB outputs with PRV-Cre

Retrograde labeling was accomplished with the use of a replication and spread-deficient Pseudorabies virus (PRV). We deleted the immediate early gene IE180, rendering the virus incapable of viral gene expression and thus viral replication or trans-neuronal spread while maintaining its ability to infect both local and retrograde neuronal populations. We engineered an IE180 null PRV strain expressing Cre-recombinase under the neuron-specific Synapsin promoter (hSyn). Virus was produced in a packaging cell line, and concentrated (titer $3.0x10^9$) using standard protocols.

The PRV-Cre virus was injected at three sites in the piriform cortex of DAT-Cre X Ai38 (ROSA-LoxP-STOP-LoxP-GCaMP3.0) mice at the following coordinates (x = lateral, y = anterior from Bregma and z = depth from the brain surface.

1. x = 2.5 mm, y = 1.8 mm and z = 4.0 mm.
2. x = 2.0 mm, y = 2.2 mm and z = 3.5 mm.
3. x = 1.5 mm, y = 2.8 mm and z = 3.0 mm.

~300 nl of virus was injected at each site.

This procedure retrogradely infected the output cells of the OB (Mitral/Tufted Cells), resulting in Cre-dependent expression of GCaMP3.0 specifically in the M/T cells. Concomitantly, to express DREADDi in DAT+ cells, we injected AAV2.9-CAG-DIO-hM4Di-mCherry in the OB as described earlier. Akin to previous experiments, this allowed DREADDi expression in DAT+ neurons. The AAV2.9 serotype was chosen to express DREADDi-mCherry in the DAT+ cells given previous results in the lab indicating lack of M/T cell infection. Each imaged brain was fixed, sagittal slices were cut and imaged via widefield epifluorescence and confocal microscopy. We found robust labeling of DREADDi-mCherry in the glomerular layer. Importantly, there was no mCherry expression in M/T cells, thereby ruling out potential leak in the M/T cells (**Figure S5C**). Two-photon imaging of M/T cell bodies was performed as described earlier for the DAT+ cells. After IP injection of CNO (5-10 mg/Kg), we waited for 30 minutes before imaging M/T odor responses for the post-CNO session.

Genetic ablation of DAT+ cells by diphtheria toxin

DAT-Cre or DAT-Cre X Thy1-GCaMP3.0 mice were injected in the OB with AAV-FLEX-DTR-GFP virus (gift from T Jessell and E. Azim, Columbia University, NYC). After 2-3 weeks post injection, either saline or Diphtheria toxin (DT, Sigma) diluted to a final amount of 400 ng in PBS was injected intraperitoneally (Azim et al., 2014). Experiments were performed at least 7 days after the induction with DT. Chronic two photon imaging was performed by implanting windows (~3 mm diameter) over the OB. Animals were imaged on DAY0 (immediately before injecting DT) and 1-2 weeks (DAYS 7-14) subsequently. In some animals,

windows were implanted on DAY 7, 1 week after injection of DT. Data from both conditions were pooled.

Optical imaging analysis

For each stimulus, a time-averaged image was separately calculated for the air and the odor periods. Baseline subtracted normalized responses (ratio images, dF/F and dR/R) were computed by subtracting the two average images and divided by the average air image. For intrinsic optical signals, the ratio image was spatially filtered, as previously described (Soucy et al., 2009). For both IOI and fluorescence imaging, to facilitate detection of responding glomeruli or cells, the ratio images were analyzed to select regions of interests (ROIs). For the sessions during which both IOI and fluorescence signals were acquired in the same animal, the intrinsic ROIs were used to extract the corresponding DAT+ cell GCaMP3.0.0 responses. In addition, random, glomerular-size (~80 μm) ROIs were selected on the OB to quantify the similarity of GCaMP3.0 responses to odors, across the bulb surface. To minimize the contribution of noise to the data, minimum response threshold was set at 1.5 sandard deviations from baseline during air period. Average odor response spectra (ORS) were calculated for each ROI to the odors in the panel.

Basic odor response properties: For each odor-ROI pair, the signal was first smoothened using a boxcar algorithm (box width - 5 frames) in Igor Pro. For each odor, the spatial spread (**Figure 1I**) of response was calculated by determining the fraction of pixels on the exposed bulb surface that responded above 2 SD from baseline average. For comparison of responses across concentrations (**Figure 1H**), responses were normalized with respect to the response at the lowest nominal dilution for each ROI-odor pair.

Lifetime Sparseness: A modified metric from Willmore and Tolhurst (Willmore and Tolhurst, 2001) was used to quantify the extent to which a given unit (glomerulus, random picked glomerular-like ROI, or DAT+ cell body) is modulated by different stimuli (**Figure S2B**). If all stimuli in the panel activate the unit rather uniformly, the lifetime sparseness measure will be close to 0; if only a small fraction of the stimuli activate the unit significantly, this metric will be close to 1.

$$LS_i = 1 - \frac{\left(\sum_{j=1}^{m} \frac{r_j}{m}\right)^2}{\sum_{j=1}^{m} \frac{r_j^2}{m}}$$

where: $m = number\ of\ odors$, $r_j = response\ of\ ROI\ A\ to\ odor\ j$

i refers to the index of the ROI A, for which lifetime sparseness is calculated.

Similarity: To quantify the overlap in response between pairs of ROIs (**Figure 1F** and **2E**), we used as a similarity metric, the uncentered correlation coefficient among their odor response spectra (ORS). Similarity between ROIs A and B:

$$S^{(A,B)} = \frac{\sum_{j=1}^{n} r_j^{(A)} \cdot r_j^{(B)}}{\sqrt{\sum_{j=1}^{n} r_j^{(A)} \cdot r_j^{(A)}} \cdot \sqrt{\sum_{j=1}^{n} r_j^{(B)} \cdot r_j^{(B)}}}$$

where

$r_j^{(A)} = response\ of\ ROI\ A\ to\ odor\ j$

$r_j^{(B)} = response\ of\ ROI\ B\ to\ odor\ j$

$n = number\ of\ odors$

Single-pixel correlation analysis: We selected glomerular-size ROIs on the exposed bulb surface as well as on the bone. From within each ROI, one single representative pixel was chosen and the normalized change in fluorescence with respect to pre-odor baseline (dF/F) was calculated averaged across repeats. Thus, for each reference pixel, we obtained a response vector of dF/F as a function of time (Reference vector, RV_0). Single pixel correlation was calculated as the correlation between RV_0 and the response vector of each pixel in the field of view.

Electrophysiology analysis

Significant spots – optogenetic mapping of DAT+ cell action: M/T units were recorded from specific sites while illuminating the bulb surface in a grid of 130 μm X 130 μm blue light spots (**Figure 3A-B**). Individual trials consisted of 500 ms of light stimulation flanked by 500 ms blank periods. Each spot was stimulated 10-15 times. Only the locations corresponding to light spots that significantly changed ('significant spots') the firing rate (FR) of the recorded unit in either direction compared to the 'pre-light' period (two-sample t-test, $p < 0.05$) were selected for subsequent analyses. The electrode position was extracted from a widefield CCD image and further used to calculate photostimulation distances from the recording site (**Figure 3B-C, S4B, Figure S5B**).Percentage inhibitory spots as a function of distance (**Figure 3C, S4B**) was calculated as the ratio of number of 'significant spots' to the total number of stimulated spots at any given distance, with a bin size of 100 μm. To determine the effect of DAT+ cell activation on M/T firing compared to chance (**Figure S4A**), the distributions of differences in spike counts were calculated across 'light on' and 'pre-light' periods, as well as across independent sets of randomly shuffled pre-stimulus periods (10,000 times, chance condition). Full width half maximum (FWHM) of a 'cold-spot' (**Figure 4D and S5B**) was calculated by fitting a 2D Gaussian distribution centered on the 2D light maps (peak normalized), with the standard deviation (sigma) as the only free parameter. Best fits were obtained using least square error method. FWHM was calculated as 2.35 times the estimated standard deviation of the fit.

Effect of photostimulating DAT+ cells on odor evoked activation of M/T units: M/T cell responses to individual odors were recorded using 15 s trials consisting of 5 s of odor presentation flanked by 5 s of air. Inter-trial intervals were varied from 15-45 s with increasing odor concentration to allow complete clearance of residual odor (as indicated by PID measurements). Odor presentations were randomly interleaved with 'odor + light' trials, where either a full-field light mask (**Figure 3D-E**) or an arbitrary combinations of glomerular-sized blue light spots (**Figure 3F-G**) were presented along with each odor. Number of spots within each pattern varied between 10 to 16 to match the average number of responsive glomeruli on the bulb surface detected via IOI. Each stimulus was repeated 7 to 10 times. M/T responses to

each odor and its corresponding 'odor + light' condition were calculated as the mean FR during the odor (or 'odor + light') periods across all repeats (**Figure 3G**). Likewise baseline FR was calculated from the air periods preceding 'odor' or 'odor + light' conditions across repeats (**Figure S4E**). In addition, for each M/T unit a significance value (p-value) was calculated for every 'odor' and 'odor + light' pair via a two-sample t-test across the repeats. To detect cell-odor pairs that were significantly modulated by light, the negative logarithm of the p-value was plotted against the logarithm of the fold change in FR between the 'odor' and 'odor + light' conditions (Volcano plot, **Figure S4F**). Significance threshold was set at $p = 0.05$. For **Figure 3D (*ii*)** and **E**, percent inhibition upon light presentation was calculated with respect to the 'odor' condition. All blue light intensities used were normalized to the maximum light intensity used for this set of experiments (7.9 mW/mm^2) and plotted in the log scale as the values varied over 3 orders of magnitude.

Halorhodopsin experiments: To ensure efficient silencing of DAT+ cell bodies and their long processes, full-field light masks were projected excluding the recording electrodes. The odor delivery conditions, trial structure and calculation of average FR during 'baseline', 'odor' and 'odor + light' were identical to the ChR2 odor experiments described above. The firing rates of M/T units were compared across 'odor' and 'odor+light' conditions and p-value evaluated (**Figure S5**). Change Index (CI) was calculated as $[(FR_{odor} - FR_{odor+light})/(FR_{odor} + FR_{odor+light})]$ where, $FR_{odor+light}$ and FR_{odor} correspond to mean absolute firing rate (spikes/s) of a given cell-odor pair during the odor period in the presence and absence of light stimulation respectively. $CI>0$ and $CI<0$ respectively indicate suppression and enhancement of firing upon light stimulation, denoting excitatory and inhibitory action of DAT+ cells respectively. Note that CI is bounded by -1 and 1, because we used absolute un-subtracted firing rates. Average CI for all cell-stimuli pairs were plotted as a function of odor-evoked firing rate binned at 2 spikes/s (**Figure 4C**).

Analysis of effects of pharmacological manipulations for ChR2 light-mapping experiments: Light mapping conditions were identical to the ChR2 experiments described earlier. For each M/T cell, we identified spots that significantly modulated the FR upon light stimulation during the drug period (two-sample t-test, $p < 0.05$; same as **Figure 3**). For each significant spot, the light induced FR change was compared in the control (pre-drug) and drug condition (**Figure 5B-C**). For a given M/T unit, we calculated the time-course of the light-induced response by computing the mean PSTH across all significant spots (**Figure 5D**). Same analysis was performed for $CdCl_2$ and APV-CNQX-BMI cocktail experiments.

Acute slice experiment analyses

Analysis was performed using the Clampfit software (Axon Instruments Molecular Devices) and custom routines in Matlab. For illustration purpose, recorded traces were *post hoc* low-pass filtered at 1 kHz (digital Butterworth filter, Matlab), and further smoothened by taking a sliding window average with a bin size of 0.5 ms. Before averaging, the baseline (mean value in 1-2 s window preceding light stimulation) was subtracted from individual traces. Few residual spikes in voltage clamp traces (1 ET cell and 1 M/T cell) recorded at -30 and -40 mV were

removed by *post hoc* thresholding. In **Figure 6B-ii** and **6D-ii**, average trace (across repeats) for each cell was normalized by the mean current in the light period in the control condition (before drug addition). The total charge was estimated (for each repeat in each cell) as the time integral of the baseline-subtracted current over the light period (**Figure S1F-H** and **6E**). This value was further corrected for the current divider effect of the series resistance (Wehr and Zador, 2003) by multiplying the current amplitude by the correction factor: $(R_{in}+R_s)/ R_{in}$, where R_s is the series resistance and R_{in} is the input resistance of the cell. R_s and R_{in} were estimated at the end of each stimulation protocol (10 trials) by measuring the current response of the cell to a square pulse of -10 mV (average of 10 repeats). R_s was estimated from the peak current of the fast capacitance transient, while $R_s+ R_{in}$ was estimated from the plateau current at the end of the pulse. Light-induced hyperpolarization was estimated as the average membrane potential during light period, following baseline subtraction (**Figure S1H** and **S8E-*iii)***.

Analyses of population imaging data

For each stimulus, response strength was calculated as a normalized change in fluorescence with respect to baseline (dF/F) averaged over all repeats. Population response strength was calculated as the mean of the response strengths to a given odor either across all the neurons in a given FOV (**Figure 7C-iii**) or across all neurons pooled from all the FOVs (**Figure 7D**). For each FOV, population response strength was calculated for each odor at 4 different concentrations as mentioned above. This yielded one concentration curve for each FOV-odor pair (n = 35 for both control and +DT). The 'best-fit-slope' was calculated by linear regression and the cumulative distribution was plotted for either conditions separately (**Figure 7F**). For each odor stimulus, the neuronal response spectrum (NRS) was defined as a vector containing the response strengths of all the recorded neurons pooled across FOVs. Population sparseness was calculated using the same formula mentioned above, with the index " i " denoting neurons. Mean population sparseness was defined as the mean of the population sparseness values across all odors (n = 5) at each concentration (**Figure 7G**). Correlation of the NRS for each odor pair was calculated. The correlation values are plotted either for all the odor pairs at 1:100 dilution (n = 10 pairs, **Figure 7H-i**) or for all the odor pairs across all the concentrations (n = 190 pairs, **Figure 7H-ii)**

References

Azim, E., Jiang, J., Alstermark, B., and Jessell, T.M. (2014). Skilled reaching relies on a V2a propriospinal internal copy circuit. Nature *508*, 357–363.

Bozza, T., McGann, J.P., Mombaerts, P., and Wachowiak, M. (2004). In vivo imaging of neuronal activity by targeted expression of a genetically encoded probe in the mouse. Neuron *42*, 9–21.

Dhawale, A.K., Hagiwara, A., Bhalla, U.S., Murthy, V.N., and Albeanu, D.F. (2010). Non-redundant odor coding by sister mitral cells revealed by light addressable glomeruli in the mouse. Nat Neurosci *13*, 1404–1412.

Soucy, E.R., Albeanu, D.F., Fantana, A.L., Murthy, V.N., and Meister, M. (2009). Precision and diversity in an odor map on the olfactory bulb. Nat Neurosci *12*, 210–220.

Wachowiak, M., Economo, M.N., Díaz-Quesada, M., Brunert, D., Wesson, D.W., White, J.A., and Rothermel, M. (2013). Optical dissection of odor information processing in vivo using GCaMPs expressed in specified cell types of the olfactory bulb. J. Neurosci. *33*, 5285–5300.

Whitesell, J.D., Sorensen, K.A., Jarvie, B.C., Hentges, S.T., and Schoppa, N.E. (2013). Interglomerular lateral inhibition targeted on external tufted cells in the olfactory bulb. J. Neurosci. *33*, 1552–1563.

Willmore, B., and Tolhurst, D.J. (2001). Characterizing the sparseness of neural codes. Network *12*, 255–270.